TUJNAS

Original Article

Thamar University Journal of Natural & Applied Sciences **9**(2) (2024) 10–15

DOI: https://doi.org/10.59167/tujnas.v9i2.2310

Electrochemical synthesis of stabilizer-free silver nanoparticles with antibacterial properties

Mohammed Ahmed Hussein Awad[1,*], Yasmin M.S. Jamil[2], and Hussein M.A. Al Maydama[2]

[1]Department of Chemistry, Faculty of Applied Science, Thamar University, Dhamar 87246, Yemen.
[2]Department of Chemistry, Faculty of Science, Sana'a University, Sana'a, Yemen.

*Corresponding author: M.A.H. Awad at Department of Chemistry, Faculty of Applied Science, Thamar University, Dhamar 87246, Yemen, E-mail: mohammed.awad@tu.edu.ye

Received: 30 September 2024. Received (in revised form): 13 November 2024. Accepted: 14 November 2024. Published: 26 December 2024.

Abstract:

In this study, we present an electrochemical method for preparing silver nanoparticles (Ag NPs) powder using a metallic silver cathode and anode in an aqueous solution of doubled distilled water (DW) with a voltage of about 27 volts. The method does not involve the use of any chemical stabilizing agents. The synthesized Ag nanoparticles were characterized using X-ray diffraction (XRD) analysis and UV-visible Spectroscopy (UV). The experiment results indicate that the crystal structure of the Ag nanoparticles sample is face-centered cubic (FCC) structure the same as the bulk materials, the crystalline size distribution ranging from 15.86 to 21.30 nm, with an average crystalline size of about 18.7 nm obtained by XRD results. Colloidal silver-NPs with a grain size of 18.7 nm were produced at optimum conditions. A peak at 406 nm was obtained in UV-visible spectroscopy attributed to Ag NPs. In addition, the synthesized Ag nanoparticles revealed a tremendous antibacterial effect against pathogenic microorganisms.

Keywords: Electrochemical Preparation; Ag Nanoparticles; XRD analysis; UV-vis spectroscopy; Antimicrobial activity.

1. Introduction

The study of silver nanoparticles has been of great scientific interest due to their physical and chemical properties, their characteristics differ depending on their size or shape. The study of Ag nanoparticles (Ag NPs) has taken various applications in medicine, catalysis, biotechnology, bioengineering, optics, and antibacterials in water treatment [1–3]. The optical properties of Ag NPs depend on their size. So many efforts are being made to synthesize Ag NPs, which are very important [4]. The effectiveness of Ag NPs as antimicrobials and antibacterials has been determined, particularly in medicine and water treatment. Antibacterial activity has been analyzed in *Streptococcus mutans*, *Staphylococcus aureus*, and *Escherichia coli*; as a result, the nanoparticles release silver ions in the bacterial cells, causing cell death of the bacteria or microbe [5–7].

For the synthesis of Ag-NP, there are several chemical and physical methods; in the chemical method, the synthesis of Ag-NP is carried out by the chemical reduction of silver salts under a reducing agent [8, 9], as that prepared by chemical reduction method using PVP (Polyvinyl pyrrolidone) [10]. In the search for environmentally friendly methods, a good option is the synthesis of Ag NPs by electrochemical reduction. The electrochemical method consists of obtaining Ag NPs formed from the reduction of a silver cathode; a main advantage of the electrochemical method is the purity of the silver particles and the possibility to control the concentration and size of the Ag NPs by varying the temperature and current density. The electrochemical method presents a limitation since the deposit of silver on the cathode during the process decreases the effective surface to produce particles. At a certain time, the production of particles ceases. Inverting the polarity at a certain time generates an anode-cathode variation with a constant voltage and avoids the deposit of silver on the cathode to obtain higher concentrations. Thus, Ag nanoparticles were synthesized in this work by reversing polarity every 60 seconds, obtaining Ag nanoparticles. The problems that the researchers in Ag NP synthesis are the complex methods of Ag NP synthesis by high prices and using more chemicals.

This search aims to prepare Ag NP powder using a fast, low-cost, and environmentally friendly electrochemical method. By applying appropriate conditions, small size, high purity, and high quantity of Ag NPs can be obtained. The Ag nanoparticles were characterized by XRD [11–15] and UV-visible Spectroscopy. The antimicrobial activity of Ag NPs was tested.

2. Experimental

2.1. Materials

Table 1: Chemicals and materials used.

Sequences	Raw materials
1	Silver electrodes with high purity reach 99.99% in dimensions (1 mm x 20 mm x 50 mm).
2	Double distilled deionized water (DW).
3	Mueller-Hinton agar (MHA, HIMEDIA, India)

2.2. Synthesis of Ag nanoparticles

The characterizations of the electrochemical method for producing nanoparticles can be described by high-purity particles and the possibility of controlling the size of the nanoparticles by controlling the current density. This method is easy and effective for producing nanoparticles without chemicals and maintains stability.

This method includes using two electrodes, anode and cathode plates made of silver with high purity, reaching 99.99%, and with dimensions (1 mm x 20 mm x 50 mm). The two electrodes are placed facing each other in a vertical way with a distance of 10 mm between each other; the set-up is placed into the electrical cell that contains 500 ml double distilled deionized water (DW). The silver particles precipitate on the cathode during the electrolysis. The electrolysis has been employed at room temperature (293 K) with continuous voltage (27.0 V), and the current passed in the circuit has been monitored with a voltmeter. Additionally, the electrical circuit has been controlled to change the Polarity between the electrodes according to the optimal period of 4 minutes. The production of nanoparticles in an electrochemical reduction manner involves changing the polarity of the direct current between the poles in addition to steering during the electrolysis process to prevent precipitation. Figure 1 shows the process of formation of colloidal silver nanoparticles in the electrochemical method as follows:

1) The oxidation of silver at the anode as shown below:

$$Ag^0 - e^- \rightarrow Ag^+ \quad (1)$$

2) The release of oxygen gas due to the electrolysis of water:

$$2H_2O - 4e^- \rightarrow O_2\uparrow + 4H^+ \quad (2)$$

At the same time, the deposition layer of Ag_2O is on the surface of the anode.

3) Immigration of the silver ions to the cathode.
4) Reduction of the ions and formation of the silver atoms on the cathode:

$$Ag^+ + e^- \rightarrow Ag^0 \quad (3)$$

The releasing of hydrogen gas during the process:

$$2H_2O + 2e^- \rightarrow H_2 + 2OH^- \quad (4)$$

5) Formation of the silver particles via the nucleation and the growth due to Van der Waals attraction.
6) Separation of the silver nanoparticles formed due to the severe steering.

In this process, the regular exchange of D.C current polarity may reduce the silver deposition rate on the cathode. During the exchange of polarity, the formed on the anode before will be hydrated during the interaction with the hydrogen gas:

$$Ag_2O + H_2 \rightarrow 2Ag + H_2O \quad (5)$$

The duration used for exchanging the polarity was 4 min. Below this time, particles would accumulate due to the gradual reduction of the surface pole's efficiency [16].

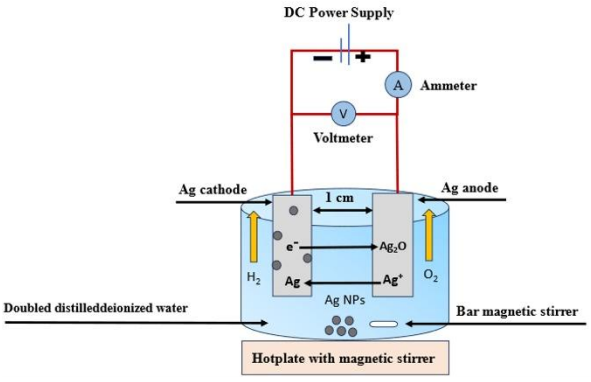

Figure 1: Illustrates the scheme of the formation of silver nanoparticles using the electrochemical method.

2.3. Physicochemical Measurements

The Ag nanoparticles were characterized by XRD (XD-2 X-ray Diffractometer) with Cu-Kα radiation (λ = 0.15418 nm; 40 kV and 40 mA). The intensity was 0-2500 counts per second (cps), and the 2 (deg) scope was 5-76 degrees. The UV-vis absorption spectrum of the prepared Ag NPs is measured using (50 conc) spectrophotometer, covering a range from (200-800) nm.

2.4. Antimicrobial activity of Ag nanoparticles

The antibacterial activity of silver nanoparticles was discovered using a well diffusion method [17,18]. Gram-negative bacteria (-) like *Pseudomonas (P.S), Escherichia coli Salmonella (S), Klebsiella (K)* and Gram-positive bacteria (+) like *Strep pyogenes (S.P)* and *Staphylococcus aureus (S.U)* were employed as microorganism strains for the antibacterial research. Sterile wells measuring 6 mm in diameter were welled on swabbed MHA plates. Various concentrations of Ag nanoparticles (100, 200, 400, and 500 mg/mL) were poured over the wells (70 μL). The negative control was sterile distilled water, and the positive control was amoxicillin. For 24 h, at 37 °C, the plates were cultured. An inhibitory zone is also detected in mm after the incubation.

3. Results and Discussion

3.1. XRD analysis

3.1.1 Structural analysis

Figure 2 shows the typical X-ray diffraction pattern for the specimen. The broad diffraction peaks suggest that the sample consists of very small particles. The major peaks of the pure Ag powders are observed. Three broad peaks with 2θ values of 38.1º, 44.4º, and 64.6º correspond to the (111), (200), and (220) planes of the bulk Ag, respectively, which can be assigned to the Ag FCC structure. The XRD pattern shows that the samples are single phase, and no other distinct diffraction peak, except the characteristic peaks of FCC phase Ag, was found [19].

From the full width at half maximum, the crystallite size for the sample can be calculated from the XRD peaks according to Scherrer formula [20-22]:

$$D_{crystallite} = \frac{K\lambda}{\beta \cos\theta} \quad (6)$$

Where $D_{crystallite}$ is the crystallite size, K = 0.89 is the Scherrer constant related to the shape and index (hkl) of the crystals, λ is the wavelength of the X-ray (Cu Ka, 1.54056 Aº), θ is the diffraction angle, and β is the corrected full width at half maximum (FWHM) (in radian). The average crystallite size (grain size) was about 18.7 nm (see Table 2).

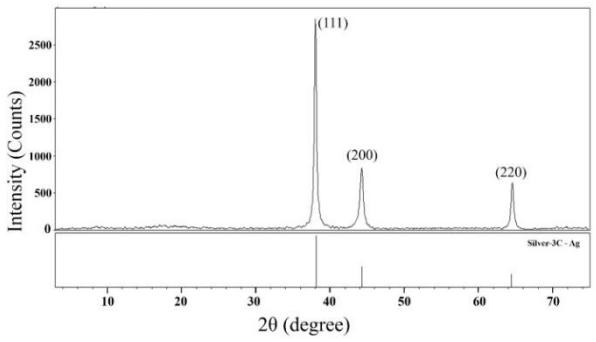

Figure 2: XRD pattern of Ag nanoparticles.

The lattice parameters (a, b, and c) for Ag nanoparticles with a face-centered cubic (FCC) crystal structure were calculated as in Table 3. The lattice parameters (a, b, and c) (Table 2) are almost identical to those reported in the (JCPDS 04-0783) card for Ag [23,24]. The d-spacing values obtained from the Braggs' law (7) and the theoretical (8) equations [25] were almost identical, as can be seen in Table 3.

$$n \times \lambda = 2d \times \sin(\theta) \Leftrightarrow d = \frac{n\lambda}{2\sin\theta} \quad (7)$$

$$1/d^2 = [(h^2 + k^2 + l^2) / a^2] \Leftrightarrow d_{hkl} = a / \sqrt{(h^2 + k^2 + l^2)} \quad (8)$$

Table 2: Crystallite size calculations of Ag nanoparticles using Scherrer's equation.

Plane (*hkl*)	(2θ)°	(θ)°	θ (rad)	cos (θ) (rad)	*β*°	*β* (rad)	D_{hkl} (nm)	D_{ave} (nm)
111	38.1	19.05	0.3324852	0.9999832	0.373	0.0065101	21.30	
200	44.4	22.2	0.3874631	0.9999771	0.501	0.0087441	15.86	**18.7**
220	64.6	32.3	0.5637413	0.9999516	0.420	0.0073304	18.92	

Table 3: Ag nanoparticles lattice parameters (a, b, and c) and the inter-planer d-spacing.

Plane (*hkl*)	2θ°	Lattice parameters (Å)		Average Volume ($V = a^3$) ($Å^3$)	d (Å) Practical	d (Å) theoretical
		A = b = c (FCC)	average			
111	38.1	4.0856	4.0794	67.8859	2.3588	2.3588
200	44.4	4.0776			2.0388	2.0388
220	64.6	4.0749			1.4407	1.4407

3.1.2 Specific surface area (SSA)

The surface area plays a critical role inside the nanoparticles due to their large surface-to-size ratio with a lower crystallite size [26]. SSA is a material property. It is a systematic value that can be used to determine a material's nature and qualities. In the context of adsorption, heterogeneous catalysis, and surface reactions, it is particularly significant. SSA stands for each mass's surface area (SA). According to Zhang's report [27], as material sizes shrink, the precise surface area and surface-to-volume ratio drastically increase. Mathematically, SSA can be computed using the following formula [28], and the calculated data are shown in Table 4.

$$SSA = 6 \times 10^3 / D\,\rho \quad (9)$$

where SSA is the specific surface area, D is the crystallite size, and ρ is the density of nanoparticles (ρ(Ag)=10.491 g cm^{-3}) [29]. Table 4 shows that the average SSA for Ag nanoparticles is 31.05 m^2 /g.

3.1.3 Dislocation density

A material's unit lattice, an atom or an ion, has a liner flaw called a dislocation. The disordering of these units in an array by some mechanisms, such as the absence of atoms or the existence of impurities, results in their dislocation. For some of the material's properties, like its mechanical and electrical properties, this flaw may be more advantageous. Industrially, these changes in lattice structure may be desired according to the resultant properties. The crystallinity of the substance is related to this lattice deformation [30].

The crystallite size and dislocation density can be computed using X-ray line profile analysis [31]. Owing to the importance of the dislocation density (δ) in the mechanical and structural properties of materials [32], it was calculated for the prepared Ag nanoparticles. The dislocation density (δ) in the sample was calculated using the expression $\delta = 1/D^2$, and the results are shown in Table 4. The δ average of Ag nanoparticles is 2.991×10^{15} m^{-2}.

3.1.4 Morphology index (MI)

It is well known that the peak broadening in the XRD pattern is due to the finite size of the particles. The width of the diffraction peaks increases with the decrease in crystallite size. The morphology index (MI) is used to affirm the uniformity and fineness of the prepared nanoparticles. It is calculated using the full width half maximum (FWHM) of the XRD peak. MI indicates that the specific surface area of Ag nanoparticles relies on the interrelationships between particle morphology and size. MI is calculated as follows: $MI = FWHM_h/(FWHM_h + FWHM_p)$ [33], where $FWHM_h$ is the highest value of full width half maximum of XRD peaks, and $FWHM_p$ is the specific value of full width half maximum of a peak where the MI has to be computed. These results are plotted in Figures 3 and 4.

The details are shown in Table 4. The MI range of Ag nanoparticles is from 0.50 to 0.573. It is discovered that MI is, with a minor variation, directly proportional to crystallite size and inversely proportional to exact surface area. The deviations and relationships between them are indicated by the linear ft within the figure. The uniformity and fitness of the prepared nanoparticles are confirmed by the MI results. Figure 5 shows that the SSA of Ag nanoparticles is inversely proportional to the crystallite size.

Table 4: Morphology Index, specific surface area, and dislocation density of Ag nanoparticles.

Plane (hkl)	2θ°	Scherrer D (nm)	Specific Surface Area (SSA) (m^2/g)	Morphology Index (MI) (unitless)	Dislocation Density (δ) (m^{-2}) × 10^{15}	Average (δ) (m^{-2})
111	38.1	21.30	26.85	0.573	2.204	
200	44.4	15.86	36.06	0.50	3.976	2.991×10^{15}
220	64.6	18.92	30.23	0.544	2.794	

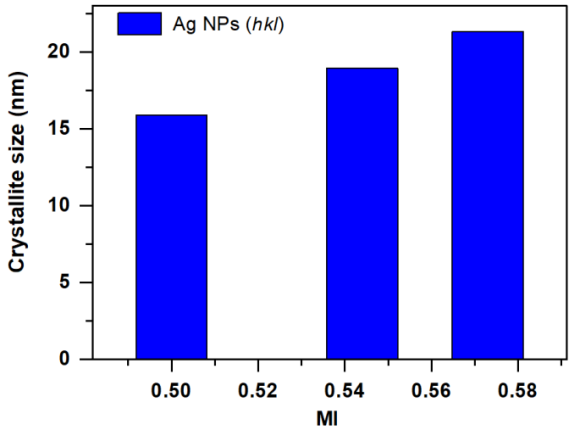

Figure 3: Morphological index vs crystallite size of Ag nanoparticles.

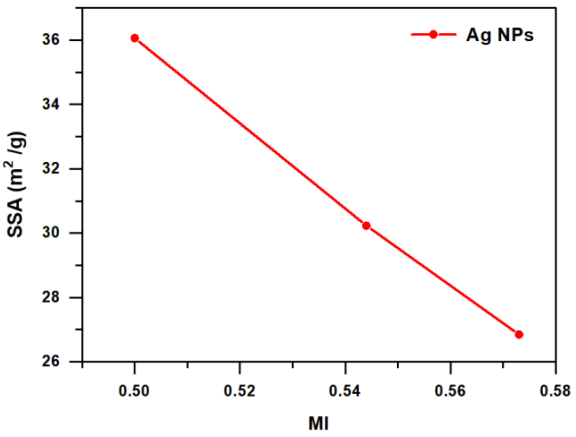

Figure 4: MI Vs specific surface area of an Ag nanoparticles (hkl).

3.2. UV-Visible spectroscopy

Plasmon bands are inimitable physical properties of nanoparticles. The surface plasmon resonance (SPR) is mostly determined by means of the dielectric properties of the metal and the surrounding medium, over and above the particle size and shape. The position of plasmon absorption bands of metallic NPs depended on the size and shape of nanostructures [34].

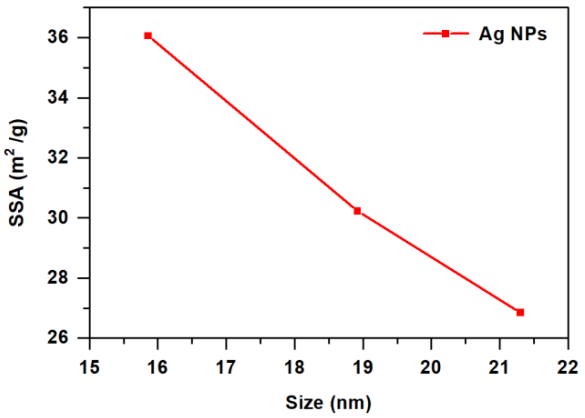

Figure 5: Size vs Specific Surface Area of Ag nanoparticles.

The optical properties of the Ag nanoparticles were investigated using the UV-VIS technique. It is well known that colloidal silver nanoparticles exhibit a broad absorption band at the wavelength from 390 to 420 nm due to Mie scattering [35,36]. The maximum absorbance observed at 406 nm is the characteristic peak of silver nanoparticle material, attributed to the localized surface plasmon resonance (LSPR) of Ag NPs [37], as shown in Figure 6. UV–VIS absorption results confirmed the formation of silver nanoparticles prepared by the electrochemical method.

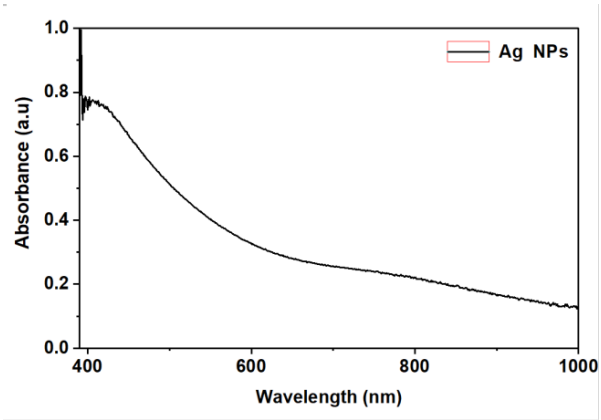

Figure 6: UV-visible spectrum of Ag NPs as a function of wavelength.

3.3. Antibacterial Activity

3.3.1 The antibacterial effect of Ag nanoparticles

Figure 7 shows the antimicrobial activity of Ag nanoparticles with concentrations (100, 200, 400, and 500 mg/mL) against *Pseudomonas (P. S)*, *Streptopyogens (S. P)*, *Escherichia coli (E. coli)*, *Salmonella (S)*, *Klebsiella (K)* and *Staphylococcus aureus (S. aureus – S.U)* bacteria (Figure 8). Synthesized nanoparticles by electrochemical methods have been found to be highly toxic against pathogenic bacteria. The antibacterial activity of silver nanoparticles can be modified with the size of silver nanoparticles, where it decreases with an increase in the particle size [38].

Table 5: Ag nanoparticles concentrations (mg/mL) and inhibition diameter (mm) of bacteria strains, the symbol (+) refers to gram-positive bacteria while the symbol (-) refers to gram-negative bacteria.

Ag NPs concentration in (mg/mL)	Inhibition zone of bacteria in (mm)					
	P.S (-)	*S.P* (+)	*E. coli* (-)	*S* (-)	*K* (-)	*S.U* (+)
100	36	30	16	26	16	16
200	38	25	15	26	14	21
400	36	28	25	34	16	26
500	38	27	17	38	15	25

After 24 hrs. of incubation, the zone of inhibition was calculated in all plates (width in mm). For six distinctive bacterial strains, gram-positive bacteria (+) and gram-negative bacteria (-), the development sector of inhibition (Table 5) was detected for some distinct concentrations of synthesized silver nanoparticles. The power of Ag NPs against the tested bacteria depended on the size and dose. The zone of inhibition in some bacteria strains increases with the increasing dose of silver nanoparticles [39]. The Ag NPs showed excellent antibacterial activity against all tested isolates, particularly against *Pseudomonas (P.S)* and Salmonella *(S)* as shown in Table 5 and Figure 8.

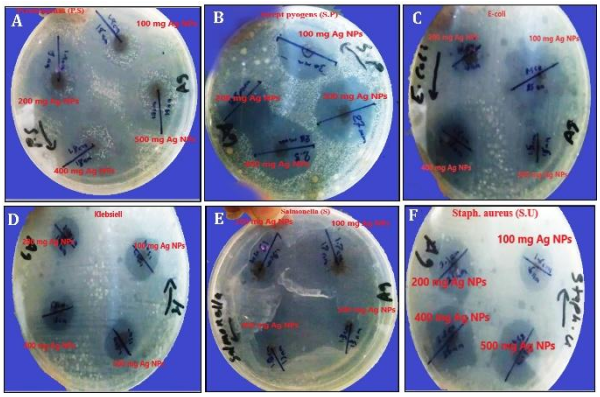

Figure 7: Antibacterial assay: zone of inhibition of Ag nanoparticles against the tested bacterial strains: (A) *Pseudomonas (P. S)*, (B) *Streptopyogens (S. P)*, (C) *Escherichia coli (E. coli)*, (D) *Klebsiella (K)*, (E) *Salmonella (S)*, and (F) *Staphylococcus aureus (S. aureus – S.U)*.

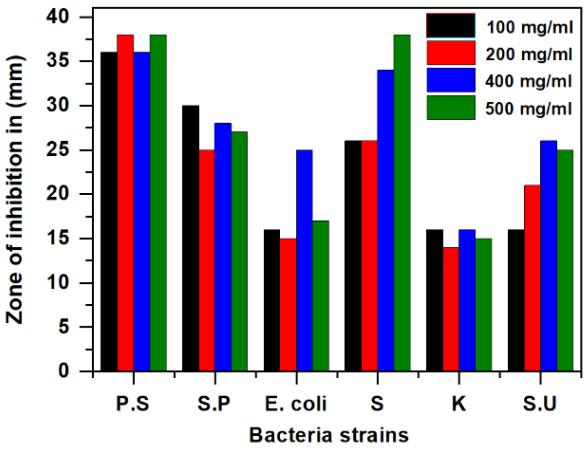

Figure 8: Comparative representation of zone of inhibition of Ag nanoparticles in diameters formed against the tested bacterial strains.

From Table 5, the antibacterial effectiveness of Ag NPs showed that *Pseudomonas (P.S)* recorded the most significant susceptibility, with inhibitory zones rising from 36 mm to 38 mm as the Ag NPs increased from 100 mg/mL to 500 mg/mL. Ag NPs' impact on *Streptpyogens (S.P)* depended on the concentration used. An inhibitory zone of 30 mm was observed at 100 mg/mL. At greater dosages of 200, 400, and 500 mg/mL, inhibitory zones measuring 25 mm, 28 mm, and 27 mm were found. The reduced inhibition at a concentration of 500 mg/mL indicates potential for nanoparticle aggregation, decreasing the surface area accessible for antibacterial action [40]. *E-coli* bacteria showed larger inhibitory zones at greater concentrations of Ag NPs. Specifically, at 400 and 500 mg/mL dosages, the zones measured 25 mm and 17 mm, respectively. The 100 and 200 mg/mL inhibition zones were 16 and 15 mm, respectively. The minor decrease in zone size as the concentration increases may be due to possible aggregation effects [40]. Concerning *Salmonella (S)* bacteria, the zone of inhibition increases with the increasing dose of silver nanoparticles. The inhibition zones of 100, 200, 400, and 500 mg/mL dosages were 26, 26, 34, and 38 mm, respectively. *Klebsiella (K)* bacteria showed the inhibition zone at 100, 200, 400, and 500 mg/mL dosages, measuring 16, 14,16, and 15 mm, respectively. A modest decrease in activity (15 mm inhibitory zone) was observed at the highest dose of 500 mg/mL, possibly due to nanoparticle aggregation reducing their effective surface area [40]. Concerning *Staph. Aureus (S.U)* bacteria, the zone of the inhibition increases with the increasing dose of silver nanoparticles. The inhibition zones of

100, 200, 400, and 500 mg/mL dosages were 16, 21, 26, and 25 mm, respectively. Ag NPs had different impacts on *Staph. Aureus (S.U) bacteria*, resulting in zone sizes of 16 mm (100 mg/mL), 21 mm (200 mg/mL), a notable increase to 26 mm (400 mg/mL), and then a decrease to 25 mm (500 mg/mL). Based on these findings, an ideal antibacterial dosage of around 400 mg/mL is recommended for combating *Staph. Aureus (S.U)* bacteria. The differences in antibacterial effectiveness shown in various bacteria may be due to variations in cell wall composition [40]. It is reported that the Ag nanoparticles with an average particle size range between 30 nm and 35 nm exhibit antibacterial activity more than some antibiotics like Ciprofloxacin 5, Vancomycin 30, and Ampicillin 10 [18]. Also, it is stated that the zone of inhibition in mm for 8 ppm concentration of Ag nanoparticles prepared by electrochemical method, with particle size between 30-70 nm, was 12 mm against *E-coli* bacteria [41]. The zone of inhibition for 100 $\frac{\mu g}{ml}$ *of* Ag NPs (average particle size between 20 to 45 nm) against *Pseudomonas* bacteria was 5 mm, and for Amoxicillin antibiotic was between 8-10 mm [42]. The zone of inhibition for 50 μg *of* Ag NPs (average particle size 29 nm) against *E. coli* bacteria was 13 mm, for *Staphylococcus aureus*, 12 mm, and for *Pseudomonas* bacteria, 17 nm, whereas for 10 µg tetracycline antibiotic, they were 10-11 mm [39].

Ag nanoparticles have inhibitive activity against tested bacteria strains because of small size of nanoparticles and their large surface area that is to say when the size of nanoparticles is small, the nanoparticles congregate on the cell surfaces and that result in increasing in their toxicity against microorganisms and that will affect on permeability of plasma membrane and result in cell death [43].

3.3.2 Antibacterial Mechanism of Silver Nanoparticles

Even though the precise mechanism of silver nanoparticles' antibacterial effects has not been completely elucidated, several antibacterial actions have been suggested. The probable antimicrobial mechanisms suggested comprise (1) Disruption of the cell wall and cytoplasmic membrane: silver ions (Ag+) released by silver nanoparticles adhere to or pass through the cell wall and cytoplasmic membrane. (2) Denaturation of ribosomes: silver ions denature ribosomes and prohibit protein synthesis. (3) Interruption of adenosine triphosphate (ATP) production: ATP production is terminated for the purpose that silver ions deactivate respiratory enzymes on the cytoplasmic membrane. (4) Membrane disruption via reactive oxygen species (ROS): reactive oxygen species generated via the broken electron transport chain can cause membrane disruption. (5) Interference of deoxyribonucleic acid (DNA) replication: silver and reactive oxygen species bind to deoxyribonucleic acid and prevent its replication and cell multiplication. (6) Denaturation of membrane: silver nanoparticles accumulate in the pits of the cell wall and cause membrane denaturation. (7) Perforation of membrane: silver nanoparticles proceed straight across the cytoplasmic membrane, which can release organelles from the cells [44].

4. Conclusion

In brief, silver nanoparticles were successfully prepared using the electrochemical method at room temperature. The crystalline structure of the particles, confirmed by XRD, is FCC structure the same as that of the bulk materials; the crystallite size ranges from 15.86 nm to 21.30 nm with an average crystallite size of about 18.7 nm. The specific surface area average and dislocation density average of Ag nanoparticles are 31.05 m^2/g and 2.991×10^{15} m^{-2}, respectively. The MI range of Ag nanoparticles is from 0.50 to 0.573. The characteristic peak in the UV-vis spectrum confirms the formation of Ag nanoparticles. Ag nanoparticles exhibited notably strong antimicrobial activity against clinical pathogenic bacteria like *Pseudomonas, Streptopyogens, Escherichia coli, Salmonella, Klebsiella,* and *Staphylococcus aureus.* Our outlook for the future of this research is to prepare Ag NPs using the electrochemical method to obtain different sizes of Ag NPs by controlling voltage and temperature.

Data Availability

The datasets used and analyzed during the current study are available from the corresponding author upon reasonable request.

Conflict of Interest

The authors declare no conflict of interest

References

[1] Ravindran, A., Chandran, P., & Khan, S. S. (2013) Biofunctionalized silver nanoparticles: Advances and prospects. *Colloids and Surfaces B: Bio interfaces* **105**: 342–352.

[2] Qassim Raheem, H., F. Hussein, E., Hameed Rasheed, A., & K. Imran, N. (2022) Antibacterial action of Silver Nanoparticles against Staphylococcus aureus Isolated from wound infection. *Research Journal of Pharmacy and Technology* **15**: 2413–2416.

[3] Khan, I., Saeed, K., & Khan, I. (2019) Nanoparticles: Properties, applications and toxicities. *Arabian Journal of Chemistry* **12**: 908–931.

[4] Tri Handoko, Chanel., Huda, Adri., and Gulo, Fakhili. (2019) Synthesis Pathway and Powerful Antimicrobial Properties of Silver Nanoparticle: A Critical Review. *Asian Journal of Scientific Research* **12**: 1-17.

[5] Liu, W.-T. (2006) Nanoparticles and their biological and environmental applications. *Journal of Bioscience and Bioengineering* **102**(1): 1–7.

[6] Rai, M., Yadav, A., & Gade, A. (2009) Silver nanoparticles as a new generation of antimicrobials. *Biotechnology Advances* **27**: 76–83.

[7] Bruna, T., Maldonado-Bravo, F., Jara, P., & Caro, N. (2021) Silver Nanoparticles and Their Antibacterial Applications. *International Journal of Molecular Sciences* **22**: 7202.

[8] Khan, Z., Al-Thabaiti, S.A., Obaid, A.Y., & Al-Youbi A.O. (2011) Preparation and characterization of silver nanoparticles by chemical reduction method. *Colloids and Surfaces B: Biointerfaces* **82**: 513–517.

[9] Vega-Baudrit, J., Gamboa, S.M., Rojas, E.R., & Martinez, V.V. (2019) Synthesis and characterization of silver nanoparticles and their application as an antibacterial agent. *International Journal of Biosensors & Bioelectronics* **5**: 166–173.

[10] Wang, H., Qiao, X., Chen, J., Wang, X., & Ding, S. (2005) Mechanisms of PVP in the preparation of silver nanoparticles. *Materials Chemistry and Physics* **94**: 449–453.

[11] Khaydarov, R.A., Khaydarov, R.R., Gapurova, O., Estrin, Y., & Scheper, T. (2008) Electrochemical method for the synthesis of silver nanoparticles. *Journal of Nanoparticle Research* **11**: 1193–1200.

[12] Rodríguez-Sánchez, L., Blanco, M.C., & López-Quintela, M.A. (2000) Electrochemical Synthesis of Silver Nanoparticles. *The Journal of Physical Chemistry B* **104**: 9683–9688.

[13] Darroudi, M., Ahmad, M.B., Abdullah, A.H., Ibrahim, N.A., & Shameli, K. (2010) Effect of Accelerator in Green Synthesis of Silver Nanoparticles. *International Journal of Molecular Sciences* **11**: 3898–3905.

[14] Saion, E., & Gharibshahi, E. (2014) On the theory of metal nanoparticles based on quantum mechanical calculation. *Malaysian Journal of Fundamental and Applied Sciences* **7**: 6 – 11.

[15] Jaimez Layna, G., Mejía García, C., Díaz Valdés, E., Guillén Cervantes, Á., Rojas Morales, M. de L., Avendaño Ibarra, M., Bautista Ramírez, M.E., & Lozano Rojas, K.J. (2024) Synthesis and characterization of silver nanoparticles by electrochemical method. *Materials Express* **14**: 1072–1077.

[16] Haider, M. J., & Mahdi, M. S. (2015) Synthesis of Silver Nanoparticles by Electrochemical Method. *Engineering and Technology Journal* **33**: 1361–1373.

[17] Arsene, M.M.J., Viktorovna, P.I., Alla, M., Mariya, M., Davares, A.K.L., Carime, B.Z., Anatolievna, G.O., Vyacheslavovna, Y.N., Vladimirovna, Z.A., Andreevna, S.L., Aleksandrovna, V.E., Alekseevich, B.L., Nikolaïevna, B.M., Parfait, K., and Andrey, V. (2023) Antimicrobial activity of Phyto fabricated silver nanoparticles using Carica papaya L. against Gram-negative bacteria. *Veterinary World* **16**: 13011311.

[18] Taqveem, H., Ur Rahman, K., Khan, S., Khan, A., Al-Ansi, W., Fahad, S., Nawaz, N., Karishma, N., Hussain, W., & Khan, L. A. (2024) Antibacterial Activity of Silver Nanoparticles Synthesized from Aloe Vera Extract. *International Journal of Environment Agriculture and Biotechnology* **9**: 54 – 61.

[19] Zhou, M., Wei, Z., Qiao, H., Zhu, L., Yang, H., & T. Xia. (2009) Particle Size and Pore Structure Characterization of Silver Nanoparticles Prepared by Confined Arc Plasma. *Journal of Nanomaterials* **2009**: 1 – 5.

[20] Jamil, Y. M. S., Awad, M. A. H., Al-Maydama, H. M. A., EL-Ghoul, Y., & Al-Hakimi, A. N. (2022) Synthesis and study of enhanced electrochemical properties of NiO nanoparticles deposited on TiO_2 nanotubes. *Applied Organometallic Chemistry* **36**: 1 – 15.

[21] Jamil, Y. M. S., Awad, M. A. H., Al-Maydama, H. M. A. (2022) Physicochemical Properties and Antibacterial Activity of Pt Nanoparticles on TiO_2 Nanotubes as Electrocatalyst for Methanol Oxidation Reaction. *Results in Chemistry* 4: 100531.

[22] Jamil, Y. M. S., Awad, M. A. H., Al-Maydama, H. M. A., Alhakimi, A.N., Shakdofa, M.M.E., & Mohammed, S.O. (2022) Gold nanoparticles loaded on TiO_2 nanoparticles doped with N_2 as an efficient electrocatalyst for

glucose oxidation: preparation, characterization, and electrocatalytic properties. *Journal of Analytical Science and Technology* **13**: 54.

[23] Pavani, K.V., Kumar, N.S., & Sangameswaran, B.B. (2012) Synthesis of Lead Nanoparticles by Aspergillus Species. *Polish Journal of Microbiology* **61**: 61–63.

[24] Gopinath, V., & Velusamy, P. (2013) Extracellular biosynthesis of silver nanoparticles using Bacillus sp. GP-23 and evaluation of their antifungal activity towards Fusarium oxysporum. *Spectrochimica Acta Part A: Molecular and Biomolecular Spectroscopy* **106**: 170–174.

[25] Shahjahan, M., Hasibur Rahman, Md., Hossain, M. S., Khatun, M. A., Islam A., & Begum, M. H. A. (2017) Synthesis and Characterization of Silver Nanoparticles by Sol-Gel Technique. *Nanoscience and Nanometrology* **3**: 34 – 39.

[26] Jiang, C., Wei, M., Qi, Z., Kudo, T., Honma, I., & Zhou, H. (2007) Particle size dependence of the lithium storage capability and high-rate performance of nanocrystalline anatase TiO_2 electrode. *Journal of Power Sources* **166**: 239–243.

[27] Gao, L., & Zhang, Q. (2001) Effects of amorphous contents and particle size on the photocatalytic properties of TiO_2 nanoparticles. *Scripta Materialia* **44**: 1195–1198.

[28] Pan, X., & Xu, Y.-J. (2013) Fast and spontaneous reduction of gold ions over oxygen-vacancy-rich TiO_2: A novel strategy to design defect-based composite photocatalyst. *Applied Catalysis A: General* **459**: 34–40.

[29] Aldayel, M.F., El Semary, N., & Adams, D.G. (2023) Differential Antimicrobial Effect of Three-Sized Biogenic Silver Nanoparticles as Broad-Spectrum Antibacterial Agents against Plant Pathogens. *Antibiotics* **12**: 1114.

[30] Jamil, S., & Fasehullah, M. (2021) Effect of Temperature on Structure, Morphology, and Optical Properties of TiO_2 Nanoparticles. *Materials Innovations* **1**: 22–28.

[31] Ungár, T., Tichy, G., Gubicza, J., & Hellmig, R.J. (2005) Correlation between subgrains and coherently scattering domains. *Powder Diffraction* **20**: 366–375.

[32] Ahmed, Abdullah A. A.., Al-Mushki, Asma. A.A., Al-Asbahi, Bandar. Ali., Abdulwahab, A. M., Abduljalil, Jameel. M.A., Saad, Fuad. A.A., Qaid, Saif. M.H. (2021) Effect of ethylene glycol concentration on the structural and optical properties of multimetal oxide CdO–NiO–Fe_2O_3 nanocomposites for antibacterial activity. *Journal of Physics and Chemistry of Solids* **155**: 110113.

[33] Othman, S.A. (2023) Characterization of Doped Titanium Dioxide (TiO_2) at Different Calcination Temperature Using X-Ray Diffraction (XRD). *ASM Science Journal* **18**: 1–8.

[34] Ahmed, Abdullah A. A., Aldeen, Thana. S., Al-Aqil, Samar. A., Alaizeri, ZabnAllah. M., and Megahed, Saad. (2022) Synthesis of Trimetallic (Ni-Cu)@Ag Core@Shell Nanoparticles without Stabilizing Materials for Antibacterial Applications. ACS Omega **7**: 37340−37350.

[35] Singh, K., Panghal, M., Kadyan, S., Chaudhary, U., & Yadav, J.P. (2014) Antibacterial Activity of Synthesized Silver Nanoparticles from *Tinosporacordifolia* against Multi Drug Resistant Strains of *Pseudomonas aeruginosa* Isolated from Burn Patients. *Journal of Nanomedicine and Nanotechnology* **5**: 192.

[36] Albashir, Mohammed. Hashim., & Mohammed, Ali. K. (2024) Influence of Stirring Time on the Electrochemical Synthesis of Silver Nanoparticles: Size and Stability Analysis. *International Journal of Research Publication and Reviews* **5**: 10065–10070.

[37] Kalainila, P., Subha, V., Ernest Ravindran, R.S., & Renganathan, Sahadevan. (2014) Synthesis and Characterization of Silver Nanoparticle from Erythrina indica. *Asian Journal of Pharmaceutical and Clinical Research* **7**: 39-43.

[38] Duque-Aristizábal, J.C., Isaza-Areiza, L.M., Tobón-Calle, D., & Londoño, M.E. (2019) Antibacterial activity of silver nanoparticles immobilized in zinc oxide-eugenol cement against Enterococcus faecalis: An in vitro study. *Revista Facultad de Odontología Universidad de Antioquia* **30**: 154–165.

[39] Nahar, Kamrun, Hafezur Rahaman, Md., Arifuzzaman Khan, G.M., Khairul Islam, Md., & Al-Reza, Sharif. M.d. (2021) Green synthesis of silver nanoparticles from *Citrus sinensis* peel extract and its antibacterial potential. *Asian Journal of Green Chemistry* **5**: 135–150.

[40] Bruna, Tamara., Maldonado-Bravo, Francisca., Jara, Paul., & Caro, Nelson. (2021) Silver Nanoparticles and Their Antibacterial Applications. *International Journal of Molecular Sciences* **22**: 7202.

[41] Sharma, Sumit., Choudhary, Kapil., Singhal, Ishu., & Saini, Rishabh. (2014) Synthesis of Silver Nanoparticles by 'Electrochemical Route' through pure metallic silver electrodes, and evaluation of their Antimicrobial Activities. *International Journal of Pharmaceutical Sciences Review and Research* **28**: 272–277.

[42] Preethi, A. Cathirin., & Krishnan, V. Harihara. (2023) The optical and electrochemical characteristics of silver nanoparticles, besides antibacterial and antifungal properties using Crocus sativus. L petals. *Research Square*, PREPRINT (Version 1) https://doi.org/10.21203/rs.3.rs-3347270/v1

[43] Lin, X., Li, J., Ma, S., Liu, G., Yang, K., Tong, M., & Lin, D. (2014) Toxicity of TiO_2 Nanoparticles to Escherichia coli: Effects of Particle Size, Crystal Phase and Water Chemistry. *PLoS ONE* **9**: e110247.

[44] Yin, Iris. Xiaoxue., Zhang, Jing., Zhao, Irene. Shuping., Mei, May. Lei., Li, Quanli., Chu, Chun. Hung. (2020) The Antibacterial Mechanism of Silver Nanoparticles and Its Application in Dentistry. *International Journal of Nanomedicine* **15**: 2555–2562.